

OncoSim: AI-PDE Modeling of Heat Diffusion for Tumor Segmentation and Thermal Therapy

Anas Mohamed

anas.bayoumi05@eng-st.cu.edu.eg

Hassan Badawy

hassan.badawy05@eng-st.cu.edu.eg

Nada Mostafa

nada.morad05@eng-st.cu.edu.eg

Saga Sadek

saga.soliman05@eng-st.cu.edu.eg

Menna Atef

menna.mahmoud06@eng-st.cu.edu.eg

Shaimaa AbdelAziz

shaimaa.ahmed05@eng-st.cu.edu.eg

Abstract—Concise Abstract: AI-PDE Framework for Precision Tumor Ablation Tumor ablation faces dual challenges: unreliable tumor boundary detection/classification and unpredictable heat spread, often causing damage to healthy tissue. Current reliance on static imaging and manual estimation is prone to error, especially with irregular tumor diffusion.

To achieve superior precision, we developed an AI-Partial Differential Equation (PDE) coupled framework. Our system first uses AI to detect, classify (malignant/benign and type), and segment the tumor from medical scans. From the segmented region, spatial features are used with a PDE tumor diffusion model to estimate the original malignant cell (tumor origin), which serves as the precise target for therapy.

The second core component is a 3D PDE-based heat diffusion model. This model dynamically simulates temperature evolution during laser ablation, allowing the system to optimize laser parameters (power, time, temperature) for safe, complete destruction limited only to the malignant area.

All functions—from scan upload, multi-segmentation, and tumor classification to thermal simulation and safety visualization—are integrated into an intuitive web-based platform. This innovative AI-PDE coupling significantly enhances the precision, safety, and interpretability of modern tumor ablation therapy.

I. INTRODUCTION

A. Problem Definition and Clinical Background

Brain tumors represent one of the most challenging neurological diseases due to their complex structure, sensitive anatomical location, and highly variable growth behavior. Among these tumors, gliomas constitute the most common primary malignant brain tumors and are associated with high morbidity and mortality rates. Despite significant advances in medical imaging and treatment technologies, accurate tumor delineation and effective therapy planning remain major clinical challenges, particularly when attempting to preserve surrounding healthy brain tissue. These challenges motivate the development of advanced, patient-specific treatment planning strategies that integrate artificial intelligence (AI) with physics-based thermal therapy modeling.

B. Overview of Brain Tumors and Glioma

Gliomas originate from glial cells, which play a supportive role in neuronal function within the central nervous system.

According to the World Health Organization (WHO), gliomas are classified into grades I–IV based on their histological and molecular characteristics. High-grade gliomas, particularly glioblastoma (WHO Grade IV), are characterized by rapid proliferation, diffuse infiltration into adjacent tissue, and poor clinical prognosis. Clinical diagnosis primarily relies on magnetic resonance imaging (MRI), which provides high-resolution structural information. However, MRI often fails to capture the true microscopic extent of tumor infiltration, leading to incomplete targeting during treatment. Owing to their aggressive growth, clear MRI appearance, suitability for laser-based thermal therapies such as laser-induced thermal therapy (LITT), and the availability of large public datasets (e.g., BraTS and TCGA), gliomas represent a suitable candidate for AI-based segmentation and therapy modeling in this study.

C. Clinical Challenges in Glioma Diagnosis and Treatment

Glioma management is complicated by several clinical challenges. First, glioma cells infiltrate healthy brain tissue, making accurate tumor boundary identification difficult. Second, conventional treatment modalities, including surgery, chemotherapy, and radiotherapy, carry a high risk of damaging critical functional brain regions. Furthermore, inter-patient variability in tumor geometry, size, and thermal response leads to non-uniform treatment outcomes. As a result, tumor recurrence remains common, with the reported median survival time for glioblastoma patients remaining approximately 12–15 months despite aggressive therapeutic intervention.

D. Limitations of Conventional Tumor Detection and Therapy Planning

Traditional tumor detection and therapy planning approaches rely heavily on manual interpretation of medical images and the use of predefined safety margins. Such methods may result in over-treatment, causing unnecessary thermal damage to healthy tissue, or under-treatment, leaving residual tumor cells untreated. In addition, these approaches lack personalization to patient-specific anatomy and tumor characteristics. In thermal and laser-based therapies, inaccurate estimation

of heat distribution further increases the risk of damaging sensitive brain regions, thereby limiting the widespread clinical adoption of these minimally invasive techniques.

E. Motivation for AI-Guided Thermal Therapy Modeling

AI-guided thermal therapy modeling provides a robust framework to overcome the limitations of conventional treatment planning for glioma therapy. This approach integrates artificial intelligence with physics-based partial differential equation (PDE) models to accurately simulate heat transfer during laser-induced thermal therapy (LITT). While PDE-based bioheat equations describe the fundamental physical processes of heat conduction and thermal diffusion within brain tissue, AI enhances these models by providing precise tumor geometry and patient-specific parameters extracted from MRI data. AI-driven segmentation enables accurate delineation of tumor boundaries, which are subsequently used to define the initial and boundary conditions of the PDE-based thermal model. Moreover, AI methods facilitate the estimation of key biological and thermal parameters, such as tissue heterogeneity, perfusion rates, and thermal conductivity, which are difficult to measure directly in clinical practice. Incorporating these parameters into the bioheat equations leads to more realistic temperature predictions and improved treatment safety and efficacy.

II. LITERATURE REVIEW

A. AI-Based Brain Tumor Detection

B. Tumor Segmentation Techniques in Medical Imaging

C. Tumor Growth and Diffusion Models

Accurately predicting the spatial spread and invasion of brain tumors remains a critical challenge in oncology, as uncontrolled tumor growth can infiltrate healthy tissue beyond MRI-visible boundaries, complicating diagnosis, treatment planning, and therapy outcomes.

1) Fisher–KPP Reaction–Diffusion Model: One of the most widely adopted mathematical formulations for modeling glioma growth in the literature is the Fisher–Kolmogorov–Petrovsky–Piskunov (Fisher–KPP) reaction–diffusion model. This model provides a biophysically interpretable description of tumor evolution by capturing two fundamental biological processes: tumor cell diffusion (invasion) and cellular proliferation.

The classical one-dimensional Fisher–KPP equation is expressed as:

$$\frac{\partial u(x, t)}{\partial t} = D \frac{\partial^2 u(x, t)}{\partial x^2} + r u(x, t) (1 - u(x, t)) \quad (1)$$

where $u(x, t)$ denotes the normalized tumor cell density, D is the diffusion coefficient representing the invasive migration of glioma cells through brain tissue, and r is the net proliferation rate governing tumor growth. The nonlinear logistic term $u(1 - u)$ accounts for growth saturation due to spatial and biological limitations.

For realistic brain tumor modeling, this formulation is commonly extended to higher spatial dimensions and rewritten in a more general form:

$$\frac{\partial c(x, t)}{\partial t} = \nabla \cdot (D \nabla c(x, t)) + \rho c(x, t) \left(1 - \frac{c(x, t)}{K}\right) \quad (2)$$

where $c(x, t)$ represents the tumor cell density at spatial location x and time t , ρ is the proliferation rate, and K denotes the carrying capacity, corresponding to the maximum packing density of tumor cells within brain tissue.

It is important to note that both equations describe the same underlying biological mechanism. The first formulation assumes a normalized cell density and one-dimensional spatial diffusion, while the second represents a generalized multidimensional version with explicit physical units and biological constraints.

Extensive studies by Swanson et al. demonstrated that this reaction–diffusion framework accurately captures the diffuse and infiltrative nature of gliomas, particularly when extended to include spatially varying diffusion coefficients that distinguish between white matter and grey matter. This enhancement significantly improves the predictive capability of the model with respect to tumor spread beyond MRI-visible regions.

As a result, the Fisher–KPP reaction–diffusion model has become the foundational mathematical model for glioma growth analysis and serves as the starting point for many advanced tumor evolution and therapy planning frameworks.

2) Reported Parameter Ranges in Glioma Modeling: Reaction–diffusion models of glioma growth rely on two key biological parameters: the diffusion coefficient D and the proliferation rate ρ . These parameters describe how tumor cells spread through brain tissue and how fast they multiply locally.

In clinical practice, direct measurement of D and ρ is not feasible. Therefore, most modeling studies adopt biologically realistic parameter ranges reported in the literature and indirectly estimated from MRI data, as described in the foundational works of Swanson et al.

Diffusion coefficient (D): The parameter D represents the invasive migration of glioma cells within the brain. Previous studies have reported that D typically lies within the range:

$$D \approx 0.001 \text{ to } 0.1 \text{ mm}^2/\text{day}.$$

Higher values of D are commonly associated with tumor spread in white matter, where tumor cells migrate more easily compared to grey matter.

Proliferation rate (ρ): The proliferation rate ρ governs the local growth of tumor cells. Reported values in the literature generally fall within the range:

$$\rho \approx 0.01 \text{ to } 0.1 \text{ day}^{-1}.$$

High-grade gliomas, such as glioblastoma multiforme (WHO Grade IV), typically exhibit larger ρ values than low-grade tumors, reflecting their aggressive biological behavior.

The ratio D/ρ as a biomarker for tumor invasiveness: Several studies have shown that the ratio D/ρ provides a simple yet powerful indicator of tumor behavior. Rather

than considering diffusion or proliferation alone, this ratio addresses a clinically important question: Does the tumor mainly spread through the brain, or does it grow locally as a compact mass?

- **Large D/ρ :** Highly diffuse tumor, spreads extensively, poorly visible on MRI, high surgical risk.
- **Small D/ρ :** Compact and localized tumor, grows mainly in place, more clearly visible on MRI, relatively easier surgical resection.

Tumors with a large D/ρ ratio tend to infiltrate surrounding brain tissue far beyond MRI-visible boundaries, making complete surgical removal difficult. In contrast, tumors with a small D/ρ ratio appear more confined, allowing for better localization and surgical planning. In this work, due to the absence of patient-specific longitudinal imaging data, parameter values were selected within the reported literature ranges, assuming a representative adult glioma patient. These assumptions provide a biologically plausible foundation for simulating tumor growth and diffusion, while acknowledging that precise personalization would require additional clinical data.

3) *Limitations of Single-PDE Models:* Although the Fisher–KPP reaction–diffusion model is widely used to describe glioma growth, relying on a single partial differential equation presents several important limitations.

First, classical reaction–diffusion models describe tumor growth using only two mechanisms: cell diffusion and cell proliferation. In reality, glioma progression is influenced by additional biological factors such as tissue heterogeneity, angiogenesis, necrosis, and treatment-induced effects. These factors cannot be fully captured by a single PDE formulation.

A key limitation of the classical Fisher–KPP model is the assumption of a spatially homogeneous diffusion coefficient. In this simplified formulation, a single constant value of the diffusion coefficient D is used, which implicitly assumes that the brain is a uniform tissue. However, the brain is not homogeneous. Experimental and clinical studies have shown that glioma cells migrate faster in white matter than in grey matter due to structural differences in brain tissue. As a result, using a single constant diffusion coefficient may oversimplify tumor invasion patterns and reduce the spatial accuracy of model predictions, unless tissue-dependent diffusion is incorporated.

Moreover, single-PDE models do not explicitly account for therapeutic interventions such as surgery, chemotherapy, or laser-based thermal therapy. Consequently, their ability to predict treatment response and post-therapy tumor evolution remains limited.

Finally, parameter estimation for these models often relies on simplified assumptions due to the limited availability of patient-specific biological and imaging data. This introduces uncertainty in model predictions, particularly when applied to individual patients.

These limitations have motivated the development of more advanced modeling frameworks that combine multiple coupled PDEs, incorporate tissue-dependent parameters, and integrate

therapy-specific physical models to achieve more realistic and clinically relevant predictions.

D. Thermal Therapy and Bioheat Models

Thermal ablation requires accurate prediction of temperature distribution. Bioheat transfer models, particularly the Pennes Bioheat Equation, are widely used to simulate tissue heating and cooling effects.

- 1) *Pennes Bioheat Equation:* This model accounts for conduction, perfusion, metabolic heat generation, and external sources, forming the basis for laser thermal therapy simulations.

E. Laser-Based Thermal Ablation Techniques

Laser interstitial thermal therapy (LITT) is a minimally invasive procedure that uses optical fibers to deliver controlled heat, necessitating precise modeling of energy deposition and heat diffusion.

F. Integration of AI and Physics-Based Models in Oncology

Combining AI for segmentation and classification with physics-based PDE simulations enables predictive modeling of tumor growth and therapeutic outcomes, paving the way for “digital twin” approaches in oncology.

G. Bioheat Transfer Models for Brain Tumor Thermal Analysis

- 1) *Introduction to Bioheat Transfer in Brain Tissues:* Thermal modeling of brain tumors represents a critical intersection in biomedical engineering. Engineering, clinical oncology, and computational physics: accurate prediction of Temperature distributions during diagnostic and therapeutic procedures require robustness. Mathematical formulations capable of accurately capturing physiological heat transfer mechanisms. As well as tumor-induced thermal heterogeneity. Over the past decades, multiple bioheat equation formulations have been proposed, each addressing specific shortcomings of earlier models.

This literature review presents a structured overview of bioheat transfer models. Applied to brain tumor thermal analysis, the review begins with the classical bioheat. The equation advances to the Pennes Bioheat Equation by incorporating the effects of blood perfusion. Extends to the Dual-Phase Lag (DPL) formulation, accounting for finite thermal wave propagation. Propagation, culminating in temperature-dependent bioheat models that accurately capture. Nonlinear variations in tissue properties at therapeutic temperatures, including relevant frameworks. Validated for laser interstitial thermal therapy (LITT). Progression reflects the increasing physiological realism required in modern contexts. Hyperthermia and thermal ablation therapies.

H. Classical Bioheat Equation

- 1) *Historical Background:* The Classical Bioheat Equation originates from Fourier’s law of heat conduction, originally formulated for homogeneous solids in the nineteenth century. Its application to biological tissues represents one of the earliest mathematical approaches to modeling heat transfer in

living systems. Despite its simplicity, the classical formulation remains useful for steady-state or slowly varying thermal processes in biological tissues.

2) Mathematical Formulation: The classical bioheat equation is expressed as:

$$\rho c \frac{\partial T}{\partial t} = k \nabla^2 T + Q(x, y), \quad (3)$$

where ρ denotes the tissue density, c is the specific heat capacity, k is the thermal conductivity, and Q represents volumetric heat generation due to metabolic activity or externally applied energy sources.

3) Applications in Brain Tumor Modeling: The classical formulation has been utilized in brain tumor thermal analysis for:

- Preliminary estimation of temperature distributions
- Baseline comparison with more advanced bioheat models
- Long-duration heating scenarios where transient effects are negligible

4) Limitations: Despite its conceptual simplicity, the Classical Bioheat Equation exhibits Several important limitations:

- Absence of blood perfusion effects
- Assumption of homogeneous and isotropic tissue properties
- Implicit assumption of infinite thermal wave propagation speed
- Inability to accurately capture rapid transient thermal responses

I. Pennes Bioheat Equation

1) Physiological Motivation: The Pennes Bioheat Equation, originally introduced in 1948, explicitly incorporates blood perfusion as a fundamental heat transfer mechanism in biological tissues [2]. Given the highly vascularized nature of brain tissue and malignant tumors, blood perfusion plays a dominant role in cerebral thermal regulation and significantly influences local temperature distributions during thermal therapies.

2) Mathematical Formulation: The Pennes bioheat equation is expressed as:

$$\rho c \frac{\partial T}{\partial t} = k \nabla^2 T + \omega_b \rho_b c_b (T_a - T) + Q_m + Q_{\text{tumor}}(x, y), \quad (4)$$

where ω_b denotes the blood perfusion rate, ρ_b and c_b represent the thermophysical properties of blood, T_a is the arterial blood temperature, Q_m is the metabolic heat generation, and Q_{tumor} accounts for tumor-induced heat sources.

3) Relevance to Brain Tumor Applications: The Pennes model effectively captures several physiologically important mechanisms:

- Enhanced perfusion levels commonly observed in malignant tumors
- Heat exchange between tissue and circulating blood
- Variations in metabolic heat generation among gray matter, white matter, and tumor tissue

Consequently, the Pennes Bioheat Equation has become the baseline thermal model in laser interstitial thermal therapy (LITT) treatment planning frameworks for simulating laser-induced temperature distributions.

4) Limitations: Despite its widespread clinical use, the Pennes model exhibits several limitations:

- Assumption of instantaneous thermal equilibrium between blood and tissue
- Spatially averaged and isotropic representation of blood perfusion
- Assumption of constant thermophysical tissue properties

J. Dual-Phase Lag (DPL) Bioheat Equation

1) Motivation Beyond Fourier Theory: The Dual-Phase Lag (DPL) bioheat model addresses the non-physical assumption of infinite thermal propagation speed inherent in classical Fourier-based heat conduction models. At short time scales and under rapid thermal excitation, biological tissues may exhibit wave-like heat transfer behavior, which cannot be accurately captured by conventional diffusion-based formulations [7].

2) Mathematical Formulation: The DPL bioheat equation is expressed as:

$$\tau_q \frac{\partial^2 T}{\partial t^2} + \frac{\partial T}{\partial t} = \alpha \nabla^2 T + \alpha \tau_T \frac{\partial}{\partial t} (\nabla^2 T) + \frac{Q(x, y, t)}{\rho c}, \quad (5)$$

where τ_q and τ_T represent the phase lags associated with the heat flux and the temperature gradient, respectively, and α denotes the thermal diffusivity of the tissue.

3) Applicability to Brain Tumor Therapies: Due to its ability to capture transient and wave-like thermal responses, the DPL model is particularly relevant for:

- Laser interstitial thermal therapy (LITT)
- Pulsed ultrasound-based thermal treatments
- Rapid heating and cooling cycles

4) Challenges: Despite its enhanced physical realism, the DPL formulation presents several challenges:

- Significant uncertainty in phase lag parameter estimation
- Increased computational complexity compared to Fourier-based models
- Limited *in vivo* experimental and clinical validation

K. Temperature-Dependent Bioheat Equation Formulations

1) Rationale for Temperature Dependence: The thermal properties of biological tissues vary significantly with temperature, particularly during hyperthermia (40–45 °C) and thermal ablation (> 50 °C) [4]. Phenomena such as protein denaturation, temperature- induced changes in blood perfusion, and water phase transitions introduce nonlinear thermal behavior that cannot be captured by a constant-parameter bioheat models.

TABLE I
COMPARISON OF BIOHEAT TRANSFER MODELS

Model	Perfusion	Transient	Cost	Clinical Use
Classical	✗	Low	Low	Educational
Pennes	✓	Moderate	Moderate	Standard
DPL	✓	High	High	Research
Temp.-Dep.	✓	Very High	Very High	LITT Planning

2) *General Temperature-Dependent Formulation:* A generalized temperature-dependent bioheat equation can be written as:

$$\rho(T)c(T)\frac{\partial T}{\partial t} = \nabla \cdot [k(T)\nabla T] + Q(T, x, y, t), \quad (6)$$

where the temperature dependence of density $\rho(T)$, specific heat capacity $c(T)$, and thermal conductivity $k(T)$ accounts for nonlinear tissue responses at elevated temperatures.

3) *Temperature-Dependent Pennes Equation:* An extended form of the Pennes bioheat equation incorporating temperature-dependent parameters is expressed as:

$$\begin{aligned} \rho(T)c(T)\frac{\partial T}{\partial t} &= \nabla \cdot [k(T)\nabla T] \\ &\quad + \omega_b(T)\rho_b c_b (T_a - T) \\ &\quad + Q_m(T) + Q_{\text{tumor}}(T, x, y), \end{aligned} \quad (7)$$

where the perfusion rate $\omega_b(T)$ and metabolic heat generation $Q_m(T)$ are explicitly modeled as temperature-dependent functions.

4) *Experimental Evidence:* Experimental and clinical studies have demonstrated that:

- Thermal conductivity increases with temperature up to approximately 45 °C and subsequently decreases during tissue coagulation
- Blood perfusion increases during mild hyperthermia and collapses at ablation temperatures
- Specific heat exhibits nonlinear variation due to protein denaturation and phase changes

5) *Clinical Significance:* Temperature-dependent bioheat models significantly improve:

- Peak temperature prediction accuracy
- Thermal lesion size estimation
- Delineation of treatment safety margins

Consequently, modern laser interstitial thermal therapy (LITT) treatment planning frameworks incorporate temperature-dependent bioheat formulations along with tissue damage metrics to enable accurate and reliable surgical simulation [5], [6], [8].

L. Comparative Summary and Model Selection

To facilitate comparison among the different bioheat transfer formulations discussed in this review, Table I summarizes their key characteristics in terms of physiological realism, computational cost, and clinical applicability.

M. Comparative Summary and Final Remarks

The evolution of bioheat transfer models for brain tumor thermal analysis demonstrates a clear trade-off between physiological realism, computational complexity, and clinical applicability. While advanced formulations such as The Dual-Phase Lag (DPL) and temperature-dependent bioheat models are capable of capturing transient wave-like heat propagation and nonlinear tissue responses, they remain computationally intensive and challenging to validate *in vivo*.

For clinical applications, particularly within AI-PDE coupled tumor ablation frameworks, the Pennes Bioheat Equation provides an optimal balance. It effectively incorporates blood perfusion and metabolic heat generation, enabling accurate temperature prediction within both the tumor and the surrounding healthy tissues while remaining computationally efficient. These characteristics make it especially suitable for real-time or near-real-time treatment planning in laser interstitial thermal therapy (LITT) and other precision thermal ablation procedures.

By integrating the Pennes model with AI-driven tumor detection, classification, and segmentation, the proposed framework can simulate heat diffusion with high fidelity while preserving healthy tissue, optimizing laser parameters, and guiding safe and precise ablation. Consequently, despite the availability of more complex Bioheat formulations, the Pennes Bioheat Equation remains the preferred choice for clinical applications that require a practical balance between accuracy, computational speed, and patient safety.

N. Summary of Research Gaps

Despite advances, challenges remain in accurately simulating heterogeneous tissue response, predicting tumor recurrence, and integrating real-time feedback into clinical workflows. Hybrid AI-PDE frameworks like OncoSim aim to address these gaps.

III. SYSTEM ARCHITECTURE AND METHODOLOGY

A. Overall BioThermoViz Framework

B. AI-Based Glioma Detection

1) *Dataset Description and Preprocessing:* In the proposed system, brain MRI images are used as the primary input for tumor analysis. Although the training phase is conducted offline, the deployed system performs standardized preprocessing to ensure compatibility with the deep learning model. Each input image is converted from OpenCV's BGR format to RGB, resized to a fixed spatial resolution of [224 × 224] pixels, and normalized to the range [0, 1] intensity range. These preprocessing steps reduce variability across images and enable consistent feature extraction during inference. The preprocessed image is then expanded along the batch dimension before being passed to the model.

2) *Model Architecture and Training Strategy:* The system utilizes a pre-trained convolutional neural network based on the VGG19 architecture for brain tumor detection and classification, employing a transfer learning strategy with offline

training on labeled brain MRI data. The VGG19 model was chosen for its high classification accuracy and efficient inference performance. In this implementation, the focus is on model deployment and inference rather than training, with an emphasis on system architecture and integration. The trained model is loaded at runtime to generate probabilistic predictions for each tumor class. To ensure system robustness, a simulation-based fallback mechanism is included for testing and demonstration purposes when the trained model or deep learning libraries are unavailable.

C. Tumor Classification and Grading

1) Tumor Type Identification: Tumor classification is performed using a pre-trained deep learning model that outputs probability scores corresponding to clinically relevant tumor categories, including glioma, meningioma, pituitary tumor, and non-tumorous tissue. The final tumor type is determined by selecting the class with the highest predicted probability.

This automated classification reduces observer dependency and supports radiologists by providing consistent and reproducible predictions. The system is designed as a decision-support tool to assist clinicians rather than replace expert interpretation.

2) Tumor Grade Prediction: After tumor classification, a rule-based clinical interpretation layer maps the predicted tumor type to an estimated grade and recommended action using predefined logic. No additional model inference is performed, and simulation outputs are clearly distinguished for testing purposes only.

This grading step does not involve additional model inference or biopsy data; instead, it directly translates the classification output into clinically meaningful information. The system clearly differentiates between AI-based predictions and simulation outputs to ensure safe and appropriate use.

D. Tumor Segmentation and Feature Extraction

Segmentation is performed to localize the spatial extent of the suspected tumor region within the brain MRI and to extract geometric features that support further clinical analysis. This stage relies on image processing and partial differential equation (PDE)-based methods rather than deep learning, enabling precise boundary delineation and robust performance.

1) Segmentation Pipeline: The segmentation process begins by converting the input MRI image to grayscale and normalizing its intensity values. A brain mask is then generated using intensity-based thresholding and morphological operations to isolate the brain region and exclude irrelevant background structures.

To reduce noise while preserving important anatomical boundaries, anisotropic diffusion filtering is applied to the brain region only. The filtered image is then segmented using multi-level Otsu thresholding to generate multiple candidate regions. Each region is evaluated using a hybrid suspicion score that combines intensity deviation from normal brain tissue and Shannon entropy, allowing abnormal regions to be identified.

The region with the highest suspicion score is selected as the initial tumor proposal and refined using a PDE-based level set method to enhance boundary accuracy. The final output of this pipeline is a binary tumor mask representing the localized tumor region.

2) Measurement of Tumor Size and Location : Following tumor segmentation, a quantitative tumor size and location measurement module was implemented to extract clinically meaningful geometric descriptors from the binary tumor mask. This feature plays a critical role in therapy planning, tumor growth model initialization, and thermal simulation setup within the BioThermoViz framework.

a) Binary Mask Normalization: The segmented tumor output is first normalized to a binary representation to ensure consistency across datasets:

$$B(x, y) = \begin{cases} 1, & \text{tumor pixel} \\ 0, & \text{background} \end{cases} \quad (8)$$

All tumor pixel coordinates are then extracted for spatial analysis.

b) Tumor Area Estimation: Tumor size is quantified by computing the total tumor area as:

$$A = N \cdot s_x \cdot s_y \quad (9)$$

where N is the number of tumor pixels and (s_x, s_y) are the MRI pixel spacing values (mm/pixel). This conversion ensures that all measurements are expressed in physical units (mm^2).

c) Bounding Box and Spatial Extent: The tumor spatial extent is characterized using a bounding box defined as:

$$x_{\min} = \min(x_i), \quad x_{\max} = \max(x_i) \quad (10)$$

$$y_{\min} = \min(y_i), \quad y_{\max} = \max(y_i) \quad (11)$$

From this bounding box, tumor width and height are computed as:

$$W = (x_{\max} - x_{\min}) \cdot s_x, \quad H = (y_{\max} - y_{\min}) \cdot s_y \quad (12)$$

d) Equivalent Circular Diameter: To provide a standardized size descriptor, the equivalent circular diameter (ECD) is calculated as:

$$\text{ECD} = 2\sqrt{\frac{A}{\pi}} \quad (13)$$

This metric enables consistent comparison of tumor size across patients and longitudinal scans, independent of tumor shape.

e) Tumor Location Estimation: Tumor location is approximated using the geometric center of the bounding box:

$$x_c = \frac{x_{\min} + x_{\max}}{2}, \quad y_c = \frac{y_{\min} + y_{\max}}{2} \quad (14)$$

This centroid estimate is sufficient for downstream applications such as laser targeting, initialization of tumor growth PDEs, and thermal source placement.

f) Shape Descriptors via Principal Component Analysis: To characterize tumor morphology, Principal Component Analysis (PCA) is applied to the spatial distribution of tumor pixels. The covariance matrix of tumor coordinates is computed as:

$$\Sigma = \text{cov}(x, y) \quad (15)$$

The eigenvalues $\lambda_1 \geq \lambda_2$ of Σ represent the major and minor axes of tumor spread, respectively:

$$a = 2\sqrt{\lambda_1}, \quad b = 2\sqrt{\lambda_2} \quad (16)$$

Using these axes, tumor eccentricity and elongation are defined as:

$$e = \sqrt{1 - \left(\frac{b}{a}\right)^2}, \quad E = \frac{a}{b} \quad (17)$$

These parameters capture tumor anisotropy and directional growth tendencies, which are particularly relevant for modeling diffusion in heterogeneous brain tissue.

g) Clinical Relevance: By converting raw segmentation masks into robust geometric and spatial descriptors—including size, location, and shape—the proposed module provides essential inputs for tumor growth modeling, laser therapy planning, and clinical decision-making. The extracted features bridge the gap between image-based segmentation and physics-based simulation within the BioThermoViz framework.

E. Tumor Growth and Diffusion Modeling

As discussed in the literature review, glioma growth is governed by a wide range of biological, anatomical, and microenvironmental factors. Modeling all these mechanisms explicitly using fully coupled multi-equation systems leads to highly complex models that are computationally expensive and difficult to personalize. In this section, we present a reduced yet biologically meaningful modeling framework that captures the dominant tumor growth dynamics while maintaining numerical tractability.

1) Biological Factors Influencing Tumor Growth: Glioma progression is influenced by several interacting biological processes. Among the most important factors affecting tumor growth and invasion are:

- **Oxygen availability:** Hypoxic conditions reduce proliferation and enhance invasive behavior.
- **Immune response:** Immune cells exert cytotoxic effects on tumor cells, effectively slowing tumor expansion.
- **Tissue heterogeneity:** Glioma cells migrate preferentially along white matter tracts, leading to anisotropic invasion patterns.
- **Genetic and molecular profile:** Mutations such as IDH status and MGMT methylation significantly affect tumor aggressiveness.
- **Edema and mechanical stress:** Tumor-induced pressure alters the tissue structure and promotes further invasion.
- **Metabolic activity:** Glucose consumption and metabolic demand regulate cell survival and necrosis.

While each of these factors can be modeled using separate governing equations, doing so results in highly coupled systems that are impractical for real-time simulation and clinical decision support.

2) Motivation for Model Reduction in Tumor Growth Modeling: Fully coupled tumor models often involve multiple partial differential equations describing tumor cell density, oxygen transport, immune dynamics, nutrient diffusion, and mechanical deformation. Although such models provide detailed biological descriptions, they suffer from several limitations:

- High computational cost due to increased dimensionality.
- Large numbers of poorly identifiable patient-specific parameters.
- Numerical stiffness requiring very small time steps.
- Limited interpretability for clinical applications.

These limitations motivate the adoption of *model reduction* strategies, in which the dominant effects of multiple processes are embedded into effective parameters of a reduced set of governing equations.

3) Model Reduction Strategy and Literature Justification: Model reduction is a well-established approach in mathematical oncology and biophysics. The central idea is to merge multiple biological and physical mechanisms into a smaller number of governing equations using biologically meaningful effective parameters. This allows preserving the dominant tumor behavior while significantly reducing model complexity.

Rather than explicitly solving separate equations for oxygen transport, immune response, and tissue mechanics, their net effects are incorporated into modified diffusion, proliferation, and decay terms of the tumor growth equation.

4) Representative Examples of Valid Model Reduction: The validity of such reduction strategies has been demonstrated in several foundational studies. In particular, Swanson et al. showed that multiple invasion mechanisms governing glioma growth can be effectively embedded into a single reaction-diffusion equation using effective diffusion and proliferation parameters. This reduced formulation successfully reproduces observed invasion fronts while remaining computationally efficient.

Similarly, the classical Pennes bioheat equation provides a canonical example of multi-physics model reduction, where heat conduction, blood perfusion, metabolic heat generation, and external energy sources are combined into a single governing equation. These examples provide strong theoretical justification for the reduced modeling approach adopted in this work.

5) Governing Equations Prior to Model Reduction: Prior to model reduction, glioma growth can be described using multiple coupled partial differential equations (PDEs), each representing a distinct biological or physical mechanism. Although these equations provide a comprehensive description of tumor dynamics, solving them explicitly requires extensive patient-specific data and leads to high computational cost. For completeness, the governing equations are presented below,

followed by simplified interpretations to clarify their physical and biological meaning.

a) 1) Tumor Cell Proliferation and Genetic Influence:

Tumor cell proliferation is commonly modeled using a logistic growth formulation:

$$\frac{\partial u}{\partial t} = \rho u(1 - u), \quad (18)$$

where $u(x, y, t)$ denotes the normalized tumor cell density and ρ is the proliferation rate. Genetic and molecular factors such as IDH mutation, MGMT methylation, and 1p/19q codeletion modify tumor aggressiveness by altering the effective values of ρ , the invasion coefficient, and necrosis rates. In the absence of patient-specific genetic data, these effects are incorporated implicitly through parameter selection within reported literature ranges.

Simplified interpretation: Equation (18) describes how tumor cells multiply locally. Growth slows down as cell density increases, reflecting biological saturation.

TABLE II
PROLIFERATION PARAMETERS FOR ADULT GLIOMA

Parameter	Meaning	Source	Typical Range
ρ	Proliferation rate	MRI / Literature	0.01–0.05 day ⁻¹

b) 2) Tumor Cell Diffusion and Tissue-Dependent Invasion: Tumor invasion into surrounding brain tissue is modeled as a diffusion process:

$$\frac{\partial u}{\partial t} = \nabla \cdot (D \nabla u), \quad (19)$$

where D represents tumor cell motility. Glioma cells migrate preferentially along white matter tracts. While diffusion tensor imaging (DTI) can capture this anisotropy, a spatially homogeneous diffusion coefficient is assumed here due to data limitations.

Simplified interpretation: This term models how tumor cells spread spatially inside the brain, similar to a diffusion process.

TABLE III
DIFFUSION PARAMETER FOR GLIOMA INVASION

Meaning (Symbol)	Source	Typical Range
Diffusion coefficient (D)	MRI / Literature	0.001–0.1 mm ² /day

c) 3) Oxygen Availability and Hypoxia Effects: Oxygen transport within the tumor microenvironment can be modeled as:

$$\frac{\partial c}{\partial t} = D_c \nabla^2 c - \lambda u c, \quad (20)$$

where $c(x, y, t)$ is the oxygen concentration, D_c is oxygen diffusivity, and λ denotes oxygen consumption by tumor cells. Hypoxia reduces proliferation, increases invasion, and promotes necrosis. These effects are embedded into effective growth and decay parameters rather than solved explicitly.

Simplified interpretation: Oxygen spreads through tissue, is consumed by tumor cells, and its shortage leads to more aggressive tumor behavior.

TABLE IV
OXYGEN-RELATED PARAMETERS

Parameter	Meaning	Source	Typical Range
D_c λ	Oxygen diffusivity Oxygen consumption	Literature Literature	100–300 mm ² /day 0.1–1.0

d) 4) Immune Response: The cytotoxic effect of immune cells on tumor tissue can be represented as a decay term:

$$\frac{\partial u}{\partial t} = -\beta u, \quad (21)$$

where β is the immune-mediated killing rate. Gliomas are known to be strongly immunosuppressive; therefore, immune dynamics are incorporated implicitly into an effective decay coefficient.

Simplified interpretation: This term accounts for tumor cell loss due to immune activity, which is generally weak in glioma.

e) 5) Edema, Pressure, and Mechanical Stress: Tumor-induced edema increases tissue pressure and enhances invasion. Mechanical effects can be modeled by:

$$\frac{\partial u}{\partial t} = -\nabla \cdot (u \nabla P), \quad P = k(u - u_0), \quad (22)$$

where P denotes tissue pressure and k is tissue stiffness.

Simplified interpretation: Pressure gradients generated by swelling push tumor cells toward surrounding tissue.

f) 6) Metabolism and Glucose Availability: Tumor metabolism influences cell survival under nutrient limitations:

$$\frac{\partial g}{\partial t} = D_g \nabla^2 g - \mu u g. \quad (23)$$

Reduced glucose availability increases necrosis and cell loss, which is reflected in an effective decay rate.

g) 7) Chemotaxis and Directed Migration: Directed migration toward favorable conditions such as oxygen or nutrients can be modeled as:

$$\frac{\partial u}{\partial t} = -\nabla \cdot (\chi u \nabla c), \quad (24)$$

where χ denotes chemotactic sensitivity.

h) Summary and Motivation for Reduction: The full tumor growth description consists of multiple coupled equations governing proliferation, diffusion, oxygen transport, immune response, metabolism, and mechanical effects. Since most of these mechanisms ultimately affect tumor diffusion, growth, or decay, their influence is consolidated into effective parameters:

$$D_{\text{eff}}, \quad \rho_{\text{eff}}, \quad \beta_{\text{eff}}.$$

This reduction preserves the dominant tumor dynamics while significantly improving numerical tractability and clinical applicability.

6) Final Combined PDE Model (Full Form): Before model reduction, tumor growth is described by a coupled system of partial differential equations that explicitly incorporates biological, mechanical, and physiological mechanisms. This formulation serves as a conceptual funnel, from which the final reduced model is derived.

a) *Tumor Cell Density Equation:*

$$\frac{\partial u}{\partial t} = \nabla \cdot (D(x, \text{genetics, age}) \nabla u - \chi u \nabla c - \delta u \nabla P) + \rho(c, \text{age, genetics, } r, M) u(1-u) - \gamma I u - \beta u \quad (25)$$

Dependent Variable:

- $u(x, y, t)$: normalized tumor cell density, $0 \leq u \leq 1$

Term-by-Term Explanation:

- $\nabla \cdot (D \nabla u)$: Tumor cell diffusion and tissue invasion. D includes white/gray matter differences, genetic aggressiveness, and age effects.
- $-\nabla \cdot (\chi u \nabla c)$: Chemotactic migration toward higher oxygen/nutrient concentration.
- $-\nabla \cdot (\delta u \nabla P)$: Pressure-driven migration due to edema and mechanical stress.
- $\rho(c, \text{age, genetics, } r, M) u(1-u)$: Logistic growth term representing proliferation with biological saturation. Includes oxygen, age, genetics, distance from core r , and metabolic factors M .
- $-\gamma I u$: Immune-mediated tumor cell killing.
- $-\beta u$: Cell loss due to hypoxia-induced necrosis and metabolic stress.

b) *Oxygen Transport Equation:*

$$\frac{\partial c}{\partial t} = D_c \nabla^2 c - \lambda u c + S_{\text{blood}}(x) \quad (26)$$

Variables:

- $c(x, t)$: oxygen concentration
- D_c : oxygen diffusivity
- λ : oxygen consumption rate by tumor cells
- S_{blood} : oxygen supply from blood perfusion

c) *Immune Cell Dynamics:*

$$\frac{\partial I}{\partial t} = \alpha u - \delta_I I \quad (27)$$

Variables:

- $I(x, t)$: immune cell density
- α : immune recruitment by tumor presence
- δ_I : immune suppression/decay

TABLE V
TYPICAL PARAMETER RANGES AND SOURCES

Meaning (Symbol)	Range	Estimation Source
Tumor diffusion (D)	0.001–0.1 mm ² /day	MRI spread
Proliferation rate (ρ)	0.01–0.05 day ⁻¹	Longitudinal MRI
Necrosis / decay (β)	0.001–0.02 day ⁻¹	Necrotic core MRI
Immune killing (γ)	< 0.01 day ⁻¹	Literature
Oxygen diffusion (D_c)	100–300 mm ² /day	Literature
Oxygen consumption (λ)	0.1–1.0	Literature
Chemotaxis strength (χ)	10 ⁻⁵ –10 ⁻³	Assumed / literature
Pressure sensitivity (δ)	10 ⁻⁴ –10 ⁻²	biomechanical models
Immune recruitment (α)	low	Literature
Immune decay (δ_I)	high	Literature

7) *Parameter Ranges and Estimation (Adult Glioma):*

8) *Clinical Interpretation:* This coupled system explicitly models tumor invasion, oxygen dynamics, immune response, and mechanical effects. However, solving it requires extensive patient-specific data, often unavailable in clinical practice.

Key intuition: Tumor growth is ultimately governed by how fast cells spread (D), proliferate (ρ), and die (β, γ). This system therefore acts as a biological funnel, motivating the construction of a reduced reaction–diffusion model with effective parameters that preserve dominant macroscopic behavior.

Sources of Parameter Values: - Tumor diffusion and proliferation rates: derived from MRI-based tumor volume evolution and literature (Swanson et al., 2000–2010). - Necrosis and immune decay: estimated from necrotic core imaging and literature. - Oxygen parameters: literature values or perfusion MRI. - Chemotaxis and pressure sensitivity: assumed or taken from biomechanical modeling studies.

9) *Numerical Solution and Implementation:* To numerically solve the tumor growth reaction–diffusion model, an Implicit-Explicit (IMEX) time integration scheme was employed. This class of methods is particularly well suited for partial differential equations that contain both stiff and non-stiff components.

a) *Motivation for IMEX Time Integration:* The governing tumor growth equation can be written in the general form:

$$\frac{\partial u}{\partial t} = D \nabla^2 u + R(u), \quad (28)$$

where the diffusion term $D \nabla^2 u$ represents spatial tumor invasion, and $R(u)$ denotes the nonlinear reaction terms, including proliferation and decay.

In this formulation:

- The **diffusion term** is **stiff**, meaning that it can change rapidly in space and time. Solving it explicitly would require very small time steps to maintain numerical stability.
- The **reaction term** is nonlinear but typically **non-stiff**, and can be treated explicitly without severe stability restrictions.

IMEX schemes address this separation by treating stiff terms implicitly and non-stiff terms explicitly.

b) *IMEX Discretization:* Using a first-order IMEX Euler scheme, the time discretization takes the form:

$$\frac{u^{n+1} - u^n}{\Delta t} = D \nabla^2 u^{n+1} + R(u^n), \quad (29)$$

where:

- u^n and u^{n+1} denote the tumor cell density at time steps n and $n+1$,
- Δt is the time step size,
- the diffusion term is treated **implicitly** to ensure stability,
- the reaction term is treated **explicitly** to avoid solving nonlinear systems.

This approach avoids the numerical instability associated with fully explicit methods, while remaining simpler and more computationally efficient than fully implicit schemes.

c) *Why IMEX Is Suitable for This Model:* The IMEX framework offers several advantages for tumor growth simulations:

- Improved numerical stability in the presence of stiff diffusion terms,
- Ability to use larger time steps compared to explicit methods,
- Reduced computational complexity compared to fully implicit solvers,
- Flexibility to incorporate additional reaction terms in future model extensions.

These properties make IMEX methods particularly appropriate for reaction–diffusion models in biological and biomedical applications.

d) *Choice of Time Integration Scheme:* During implementation, both implicit and explicit time integration schemes were tested. While fully implicit methods provided higher numerical accuracy, they required solving nonlinear systems at each time step, significantly increasing computational cost.

For practical implementation within an interactive visualization application, A first-order Euler-based IMEX scheme was selected. Although Euler integration is less accurate than higher-order methods, but it offers:

- Fast computation,
- Simple implementation,
- Sufficient precision for qualitative visualization of tumor growth.

Given the real-time performance requirements of the application, the Euler IMEX scheme provided the best balance between numerical stability, accuracy, and computational efficiency.

e) *Summary:* In summary, the tumor growth model was solved using an IMEX Euler time integration scheme, where diffusion is handled implicitly and reaction terms explicitly. This choice ensures stable numerical behavior, computational efficiency, and suitability for real-time tumor growth simulation.

F. Laser-Based Thermal Ablation Techniques

1) *Optical Interaction and Wavelength Selection:* The efficacy of laser ablation is fundamentally dependent on the interaction between light and tissue, which varies significantly by wavelength. Prior investigations into the optical properties of brain tissue have measured the absorption coefficients (μ_a) and scattering coefficients (μ_s) to determine optimal laser parameters.

Research indicates that specific wavelengths offer distinct advantages depending on the depth of the target lesion:

- **810 nm:** Studies suggest this wavelength exhibits a lower absorption coefficient ($\mu_a \approx 0.08 \text{ mm}^{-1}$), allowing for deeper penetration into the tissue, making it suitable for larger, deep-seated lesions.
- **980 nm:** Has been shown to have higher water absorption, leading to more localized heating but shallower penetration.

• **1064 nm (Nd:YAG):** Often cited as a standard wavelength in neurosurgery, offering a balance between penetration depth and thermal absorption.

2) *Artificial Intelligence and Predictive Control:* Given the rapid thermodynamics of laser ablation, relying solely on human reaction or reactive feedback loops has been identified as a safety risk. Recent literature emphasizes the integration of **Artificial Intelligence (AI)** and **Machine Learning (ML)** algorithms to enhance surgical precision.

Researchers have proposed “intelligent” control systems that do not merely react to current temperatures but actively forecast future thermal states. By analyzing the temporal derivative of temperature (dT/dt) and using predictive modeling (such as Kalman filters or linear regression), these AI agents can mitigate system latency inherent in MRI thermometry.

A common predictive control algorithm discussed in biomedical engineering literature uses a look-ahead projection to prevent carbonization (charring) and explosive vaporization (“steam pops”):

$$T_{predicted}(t + \Delta t) = T_{current}(t) + \left(\frac{dT}{dt} \right)_{avg} \times \Delta t \quad (30)$$

By projecting the temperature trend forward (typically by 5–10 seconds), AI-driven controllers can preemptively modulate laser power, ensuring the tissue temperature remains within the safety corridor before a critical violation occurs.

3) *Clinical Thresholds for Glioblastoma:* Clinical reviews regarding high-grade gliomas, specifically Glioblastoma (GBM), have established specific thermal dose requirements for effective treatment. Unlike benign tissue, malignant glioma cells have demonstrated resistance to lower thermal doses.

Consensus in the medical community suggests that a target temperature range of **60°C to 65°C** is required to ensure irreversible coagulative necrosis in the tumor core. Simultaneously, protecting the surrounding healthy parenchyma is critical; studies define the safety margin threshold at **43°C**, above which the risk of permanent neurological deficit increases significantly.

G. Laser Therapy Parameter Calculation

Laser therapy parameters are initially estimated using a physics-based model that accounts for tumor geometry, depth, and wavelength-dependent optical properties of brain tissue. The objective is to determine the required laser energy, power, and exposure duration to raise tumor temperature to cytotoxic levels while respecting clinical safety constraints.

1) *Wavelength-Dependent Optical Absorption:* Laser-tissue interaction is modeled using wavelength-specific absorption coefficients of brain tissue. Since optical absorption varies significantly with wavelength, a discrete set of absorption coefficients derived from biomedical optics literature is used to approximate tissue behavior for common medical laser wavelengths (e.g., diode, Nd:YAG, and CO₂ lasers).

For a given laser wavelength, the absorption coefficient μ_a is selected based on the closest available wavelength in

the predefined dataset, ensuring realistic modeling of light attenuation in tissue.

2) *Laser Energy Deposition (Beer–Lambert Law)*: The attenuation of laser intensity with tissue depth is described by the Beer–Lambert law:

$$I(z) = I_0 e^{-\mu_a z} \quad (31)$$

where $I(z)$ is the laser intensity at depth z , I_0 is the incident surface intensity, μ_a is the absorption coefficient of brain tissue, and z is the tumor depth.

In this work, the equation is used inversely: for a known tumor depth, the required surface intensity I_0 is estimated to ensure sufficient heating at the tumor core.

3) *Energy and Power Estimation*: The thermal energy required to raise tumor temperature from baseline body temperature (37°C) to a therapeutic target temperature (typically 65°C) is estimated using classical heat transfer principles:

$$Q = mc\Delta T \quad (32)$$

where the tumor mass m is derived from its estimated spherical volume, c is the specific heat capacity of tissue, and ΔT is the desired temperature rise.

The required energy is adjusted by a penetration factor to compensate for depth-dependent optical attenuation. A standard exposure duration is initially assumed, and laser power is computed accordingly. To ensure clinical safety, laser power is capped at a maximum allowable value. This physics-based calculation provides an initial estimate of laser power, energy, duration, and target temperature for subsequent thermal simulation and control.

IV. AI-GUIDED MONITORING AND TREATMENT PLANNING

An integrated AI-based framework is employed to support both treatment planning and real-time thermal monitoring during laser ablation. The system combines preoperative parameter estimation with intraoperative adaptive control to ensure effective tumor destruction while minimizing damage to surrounding healthy tissue.

A. AI-Assisted Treatment Planning

Prior to ablation, an AI-assisted treatment planning module generates initial laser parameters based on tumor size and pathological type. Smaller lesions are assigned lower power and energy levels to reduce unnecessary thermal spread, whereas larger tumors require higher power and longer exposure durations to achieve a sufficient thermal dose.

Tumor pathology further refines the treatment plan. Malignant tumors are assigned higher target temperatures (up to 65°C) to ensure cytotoxic heating, while benign tumors are treated at lower target temperatures (approximately 55°C). These parameters serve as initial guidelines rather than fixed values, allowing further refinement during the ablation procedure.

B. AI-Guided Monitoring Workflow

During ablation, an AI-driven monitoring module provides continuous supervision of tissue temperature and laser–tissue interaction through a closed-loop control workflow, as illustrated below.

1) *Data Acquisition and Temperature Smoothing*: A rolling buffer stores the most recent temperature measurements (up to 10 samples). A rolling average filter is applied to reduce sensor noise and provide a stable and reliable estimate of tissue temperature for downstream analysis.

2) *Heating Rate Estimation*: The temporal temperature gradient (dT/dt) is computed from consecutive temperature measurements. This metric enables early detection of rapid temperature increases that may indicate unsafe heating conditions or the onset of thermal runaway.

3) *Predictive Temperature Analysis*: Using the smoothed temperature and estimated heating rate, the system predicts future tissue temperature over a short time horizon. This predictive capability allows proactive intervention before critical thermal thresholds are exceeded.

4) *Safety Threshold Evaluation*: Multiple safety criteria are continuously evaluated, including:

- Maximum allowable temperature at the tumor centroid.
- Thermal exposure at the tumor margin and surrounding healthy tissue.
- Sudden impedance spikes indicative of tissue charring or carbonization.

Margin temperatures exceeding 42°C trigger a warning state, while temperatures above 45°C result in immediate system shutdown to prevent irreversible damage to healthy tissue.

5) *Decision Making and Control Actions*: Based on the current and predicted thermal state, the AI dynamically selects an appropriate control action. These actions include continuing heating under stable conditions, boosting power during inefficient heating, reducing power near the target temperature, pausing the procedure to allow thermal stabilization, or triggering an emergency stop when critical safety limits are violated.

6) *Closed-Loop Feedback Control*: This monitoring and control cycle is executed continuously in real time, forming a closed-loop feedback system that adapts laser delivery to patient-specific thermal behavior. The closed-loop architecture ensures safe, precise, and effective tumor ablation while minimizing collateral damage to surrounding healthy brain tissue.

C. Thermal Ablation Simulation

To model laser-induced heating and tissue response, a reduced-order thermal ablation model is employed. The model tracks temperature evolution at two characteristic locations—the tumor centroid and tumor margin—using a simplified formulation of the Pennes bioheat equation.

1) *Governing Bioheat Equation*: The thermal behavior of tissue is governed by the Pennes bioheat equation:

$$\rho c_p \frac{\partial T}{\partial t} = \nabla \cdot (k \nabla T) + Q_{\text{laser}} + Q_{\text{met}} - \omega_b \rho_b c_b (T - T_a) \quad (33)$$

where ρ is the tissue density, c_p is the specific heat capacity, k is the thermal conductivity, ω_b is the blood perfusion rate, ρ_b and c_b are the blood density and specific heat, and T_a is the arterial blood temperature. Metabolic heat generation Q_{met} is considered negligible and is omitted for real-time simulation.

2) *Reduced-Order Two-Point Approximation*: To enable fast and stable simulation suitable for real-time applications, the full three-dimensional PDE is reduced to a two-point model:

- **Centroid temperature** $T_c(t)$: represents the hottest region near the laser tip.
- **Margin temperature** $T_m(t)$: represents the tumor boundary adjacent to healthy tissue.

This approach preserves the dominant thermal dynamics while significantly reducing computational cost.

3) *Centroid Temperature Evolution*: The centroid temperature evolves according to:

$$\frac{dT_c}{dt} = \frac{P}{\rho c_p V_{\text{eff}}} - \frac{\omega_b(T_c)\rho_b c_b}{\rho c_p}(T_c - T_a) - \frac{k}{\rho c_p L_{\text{eff}}}(T_c - T_m) \quad (34)$$

where P is the laser power, V_{eff} is the effective optical penetration volume, and L_{eff} is the effective conduction length.

This equation models laser heating, temperature-dependent perfusion cooling, and thermal conduction from the centroid to the tumor margin. An explicit Euler forward scheme is used to update the centroid temperature at each time step.

4) *Temperature-Dependent Perfusion Model*: Blood perfusion is modeled as a function of temperature:

$$\omega_b(T) = \begin{cases} \omega_0, & T \leq 37^\circ\text{C} \\ \omega_0 [1 + \alpha (1 - e^{-\beta(T-37)})], & 37 < T \leq 60^\circ\text{C} \\ 0, & T > 60^\circ\text{C} \end{cases} \quad (35)$$

This formulation captures physiological vasodilation at moderate temperatures and vascular shutdown following thermal coagulation.

5) *Margin Temperature Estimation*: The tumor margin temperature is approximated using a Gaussian-like spatial decay:

$$T_m = T_a + (T_c - T_a) \cdot 0.45 \cdot \frac{1}{1 + 0.1\sqrt{A_{\text{tumor}}}} \quad (36)$$

where A_{tumor} represents the tumor cross-sectional area. This expression accounts for heat attenuation with tumor size, ensuring that larger tumors exhibit cooler margins due to increased conduction distance.

6) *Ablation Criterion*: Thermal damage is assessed using a threshold-based criterion suitable for real-time monitoring:

$$\text{is_destroyed} = (T_c \geq T_{\text{target}}) \text{ or } (T_m \geq T_{\text{target}}) \quad (37)$$

Typical target temperatures range between 60 °C and 70 °C. While cumulative damage models such as the Arrhenius integral are well established, they are not employed here due to their high computational cost and limited suitability for real-time control.

D. Summary

By integrating physics-based laser parameter estimation with a reduced-order thermal ablation model, the proposed framework achieves a balance between physical accuracy and computational efficiency. This approach enables patient-specific treatment planning, real-time thermal prediction, and safe laser therapy execution while preserving surrounding healthy brain tissue.

V. APPLICATION WORKFLOW AND USER INTERFACE

A. Application Initialization and Model Availability Check

Upon launching the application, the system performs an automatic initialization routine to verify the availability of the required artificial intelligence (AI) inference environment. Specifically, it checks whether the deep learning framework and the pre-trained convolutional neural network (CNN) model for tumor classification are properly loaded and operational.

This step ensures robust execution and allows the application to seamlessly proceed with image analysis without user intervention. The classification model is designed to operate in real time, enabling rapid assessment of incoming medical images.

B. Tumor Detection, Classification, and Segmentation

After successful initialization, the clinician uploads a brain MRI scan to the application. The system first performs tumor presence detection to determine whether malignant tissue is present. If a tumor is detected, the AI-based classifier identifies the tumor category, providing an initial diagnostic assessment.

Subsequently, a dedicated segmentation pipeline is executed to localize the tumor region within the image. The segmentation stage produces a binary tumor mask that accurately delineates tumor boundaries, which serves as the foundation for all subsequent modeling and simulation steps.

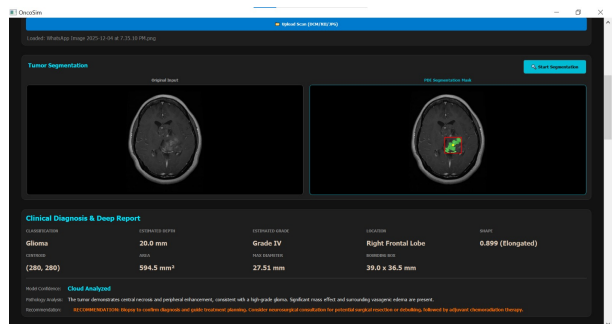


Fig. 1. Tumor detection, classification output, and segmentation mask overlay.

C. Tumor Size, Location, and Feature Extraction

Following segmentation, the application automatically extracts clinically relevant tumor features from the binary mask. These include tumor area, spatial extent, equivalent diameter, centroid location, and shape descriptors such as eccentricity and elongation.

These quantitative features are displayed within the Clinical Diagnosis section of the application and are directly used to initialize both tumor growth modeling and thermal therapy simulations, effectively bridging image-based diagnosis with physics-based prediction.

D. Laser Therapy Parameter Recommendation and Thermal Simulation

Based on the extracted tumor features, the application proposes an initial set of laser ablation parameters, including laser power, exposure duration, and target temperature. These parameters are estimated using the bioheat and energy deposition equations described earlier in this paper.

The clinician may manually adjust the initial tissue temperature and laser settings before starting the ablation simulation. Once initiated, the system solves the governing bioheat PDE to generate a spatial temperature distribution that visualizes laser-induced heat diffusion within the tumor and surrounding tissue.

To ensure patient safety, predicted temperatures in healthy tissue are continuously monitored. If excessive thermal damage outside the tumor boundary is expected, a warning alert is issued.

E. Tumor Growth Prediction Using PDE-Based Modeling

In addition to thermal therapy planning, the application includes a tumor growth prediction module based on reaction-diffusion PDE modeling. The user can configure key biological parameters and select between a fast simulation mode for rapid assessment or an accurate mode for higher numerical resolution.

The tumor growth equation is solved numerically using an Euler-based IMEX time integration scheme, enabling stable simulation of diffusion-driven invasion and nonlinear proliferation. Predicted tumor expansion is visualized dynamically, providing real-time insight into future tumor progression and estimated growth rates.

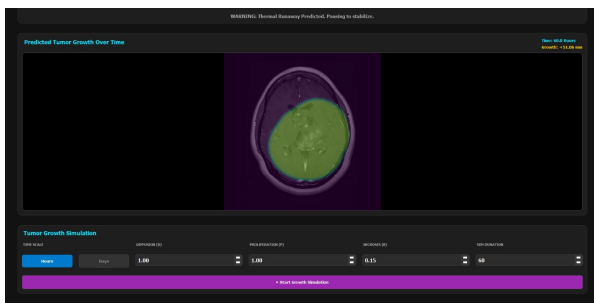


Fig. 2. PDE-based tumor growth prediction visualized over time.

F. AI-Assisted Clinical Interpretation Interface

The system leverages AI to analyze segmented tumor regions and extracted features through a standardized API, generating structured clinical interpretations including tumor

aggressiveness, size, spatial extent, and potential clinical implications. An interactive chat interface allows clinicians to request clarifications on tumor morphology, progression trends, thermal therapy planning, and other imaging-based insights. This tool is strictly for clinical decision support, ensuring full clinician oversight and accountability while improving usability and interpretability.

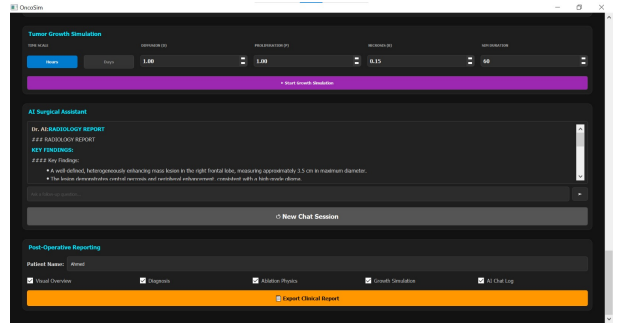


Fig. 3. Overview of AI-assisted clinical interpretation interface.

G. Automated Report Generation

Finally, the application provides an automated medical report generation module that summarizes all stages of analysis performed within the system. The generated report includes tumor detection results, classification outcomes, segmentation maps, quantitative tumor measurements, tumor growth prediction outputs, and thermal ablation simulation findings.

To support different clinical and research workflows, clinicians can selectively choose which sections to include in the final report. This flexibility enables the generation of concise clinical summaries or more detailed technical reports, depending on the intended use case.

H. Summary

This end-to-end application workflow demonstrates the tight integration of AI-driven medical image analysis with PDE-based physical modeling within a single interactive platform. By unifying tumor detection, quantitative analysis, growth prediction, and thermal therapy simulation, the proposed system provides a practical and clinically interpretable tool for precision tumor diagnosis and treatment planning.

VI. CONCLUSION

OncoSim presents a compact AI-PDE framework for precise tumor segmentation and laser-based thermal therapy. By combining deep learning–driven tumor detection with PDE-based tumor growth and heat diffusion models, it enables accurate tumor localization and safe thermal planning. The system supports clinicians with real-time simulations, preserving healthy tissue while optimizing therapy parameters. This integrated approach demonstrates significant potential for personalized, precise, and interpretable tumor ablation.

VII. FUTURE WORK

A. 3D Volumetric Modeling

The current implementation operates on two-dimensional (2D) MRI slices. A natural extension of this work is to develop partial differential equation (PDE) solvers capable of handling full three-dimensional (3D) volumetric data obtained from NIfTI or DICOM image stacks. Such an extension would enable more realistic simulations of heat diffusion and tumor growth by explicitly accounting for spatial interactions along the Z-axis, thereby improving anatomical fidelity.

B. Integration of Patient-Specific Tissue Properties

At present, the model relies on generalized literature-based values for tissue parameters such as thermal conductivity, density, and blood perfusion. Future work may focus on incorporating patient-specific tissue properties derived from advanced MRI modalities, including perfusion-weighted imaging and diffusion imaging. This enhancement would facilitate the creation of a personalized thermal and biological *digital twin*, enabling more accurate treatment planning and outcome prediction.

REFERENCES

- [1] American Cancer Society, “Brain and Spinal Cord Tumors in Adults,” [Online]. Available: <https://www.cancer.org/cancer/types/brain-and-spinal-cord-tumors-adults.html>. Last updated Jan. 2023. Accessed Sep. 3, 2025.
- [2] Canadian Cancer Society, “Chemotherapy for brain and spinal cord tumours,” [Online]. Available: <https://cancer.ca/en/cancer-information/cancer-types/brain-and-spinal-cord/treatment/chemotherapy>. Last updated Jan. 2023. Accessed Sep. 3, 2025.
- [3] F. B. Mesfin and M. A. Al-Dahir, “Gliomas,” in *StatPearls [Internet]*, Treasure Island, FL: StatPearls Publishing, Jan. 2024–. 2023 May 20. [Online]. Available: <https://www.ncbi.nlm.nih.gov/books/NBK441874/>. Accessed Sep. 3, 2025.
- [4] National Organization for Rare Disorders (U.S.), “Glioma,” [Online]. Available: <https://rarediseases.org/rare-diseases/glioma/>. Last updated Aug. 5, 2024. Accessed Sep. 3, 2025.
- [5] S. H. Torp, O. Solheim, and A. J. Skjulsvik, “The WHO 2021 Classification of Central Nervous System tumours: a practical update on what neurosurgeons need to know—a minireview,” *Acta Neurochirurgica (Wien)*, vol. 164, no. 9, pp. 2453–2464, Sep. 2022. [Online]. Available: <https://pmc.ncbi.nlm.nih.gov/articles/PMC9427889/>. Accessed Sep. 3, 2025.
- [6] “Integrating forecasting methods to support finite element analysis and explore heat transfer complexities,” Academic Hosting & Event Management Solutions. [Online]. Available: <https://www.ncbi.nlm.nih.gov>.
- [7] “Glioblastoma Multiforme: A Review of its Epidemiology and Pathogenesis through Clinical Presentation and Treatment,” [Online].
- [8] “Laser Ablation for Gliomas,” IntechOpen, [Online].
- [9] K. R. Swanson, E. C. Alvord, and J. D. Murray, “A quantitative model for differential motility of gliomas in grey and white matter,” *Cell Proliferation*, vol. 33, no. 5, pp. 317–329, 2000.
- [10] K. R. Swanson, E. C. Alvord, J. D. Murray, and F. E. Dale, “Virtual brain tumours (gliomas) enhance the reality of medical imaging,” *British Journal of Cancer*, vol. 86, no. 1, pp. 14–18, 2002.
- [11] T. Hillen and K. J. Painter, “Transport and anisotropy in glioma invasion,” *Journal of Mathematical Biology*, vol. 67, no. 4, pp. 911–943, 2013.
- [12] L. G. de Pillis, A. E. Radunskaya, and C. L. Wiseman, “A validated mathematical model of cell-mediated immune response to tumor growth,” *Cancer Research*, vol. 66, no. 17, pp. 8503–8513, 2006.
- [13] H. H. Pennes, “Analysis of tissue and arterial blood temperatures in the resting human forearm,” *Journal of Applied Physiology*, vol. 1, no. 2, pp. 93–122, 1948.
- [14] H. B. Frieboes, J. S. Lowengrub, S. M. Wise, X. Zheng, and V. Cristini, “Three-dimensional multispecies nonlinear tumor growth – II: Tumor invasion and angiogenesis,” *Journal of Theoretical Biology*, vol. 264, no. 4, pp. 1254–1278, 2010.
- [15] “Optical Properties: Optical Properties and Fluence Distribution in Head Tissues at Selected Laser Wavelengths,” *Journal of Biomedical Photonics & Engineering*, [Online].
- [16] “AI & Control: Model-based planning and real-time predictive control for laser-induced thermal therapy,” PMC / ResearchGate, [Online].
- [17] “Clinical Safety: Laser Interstitial Thermal Therapy for Glioblastoma: Safety, Efficacy, and Outcomes,” *MDPI Cancers*, PubMed Central, [Online].
- [18] A. Mohammadi, L. Bianchi, S. Asadi, and P. Saccomandi, “Measurement of ex vivo brain thermal properties,” *Sensors*, vol. 21, no. 12, Art. no. 4236, 2021. [Online]. Available: <https://www.mdpi.com/1424-8220/21/12/4236>.
- [19] H. H. Pennes, “Analysis of tissue and arterial blood temperatures in the resting human forearm,” *J. Appl. Physiol.*, vol. 1, no. 2, pp. 93–122, 1948. [Online]. Available: <https://journals.physiology.org/doi/10.1152/jappl.1948.1.2.93>.
- [20] M. Farrell et al., “Computational modeling of photon transport and tissue heating during transcranial near-infrared stimulation,” *Brain Sciences*, vol. 9, no. 8, Art. no. 179, 2019. [Online]. Available: <https://www.mdpi.com/2076-3425/9/8/179>.
- [21] C. Rossmann and D. Haemmerich, “Review of temperature dependence of thermal properties, dielectric properties, and perfusion of biological tissues at hyperthermic and ablation temperatures,” *Crit. Rev. Biomed. Eng.*, vol. 42, no. 6, pp. 467–492, 2014. [Online]. Available: <https://pubmed.ncbi.nlm.nih.gov/25500057/>.
- [22] A. El-Baz et al., “Modeling and in vivo experimental validation of 1,064nm laser interstitial thermal therapy on brain tissue,” *Front. Neurol.*, 2023. [Online]. Available: <https://www.frontiersin.org/articles/10.3389/fneur.2023.1237394/full>.
- [23] M. H. Ebrahimi et al., “Treatment Modelling of a 3D Tumour in Brain by Laser-Induced Interstitial Thermotherapy,” *J. Lasers Med. Sci.*, 2020. [Online]. Available: <https://journals.sbm.ac.ir/jlms/article/view/40102>.
- [24] F. D. Lee et al., “Modeling for neurosurgical laser interstitial thermal therapy with and without intracranial recording electrodes,” *Int. J. Hyperthermia*, 2021. [Online]. Available: <https://www.sciencedirect.com>.
- [25] S. Balasubramanian et al., “Development of a Treatment Planning Framework for Laser Interstitial Thermal Therapy (LITT),” *Cancers*, vol. 15, no. 18, 2023. [Online]. Available: <https://doi.org/10.3390/cancers15184554>.